#6940

An Analysis of Moisture Accumulation in a Wood-Frame Wall Subjected to Winter Climate

D.M. Burch **W.C. Thomas**

ABSTRACT

A transient, one-dimensional, finite-difference model is presented that predicts the coupled transfer of heat and moisture in a multilayer wall under nonisothermal conditions. The model can predict moisture transfer in the diffusion through the capillary flow regimes. It has a provision to account for convective moisture transfer by including embedded cavities that may be coupled to indoor and outdoor air.

The model is subsequently used to predict the time-varying average moisture content in the sheathing and siding of a wood-frame wall as a function of time of year. Results are shown for a mild winter climate (Atlanta, Ga.), an intermediate winter climate (Boston, Mass.), and a cold winter climate (Madison, Wis.). The indoor temperature is maintained at 21°C, and separate computer runs are carried out for indoor relative humidities of 35% and 50%.

The effect of several construction parameters on the winter moisture accumulation is investigated. The parameters include the interior vapor retarder permeance, sheathing permeance, exterior paint permeance, indoor air leakage, and the amount of insulation.

INTRODUCTION

During the winter season, the absolute humidity (or moisture content) of the air within a residence is considerably higher than that of the outdoor air. As a result, moisture permeates into walls by way of diffusion and air leakage through cracks in the interior surface. This moisture is partially adsorbed and accumulates within the outer material layers of the wall. In response to the seasonal variation in outdoor temperature, Duff (1968) observed that the moisture content in outer wall layers builds up during cold winter periods and subsequently decreases during warm summer periods.

Seasonal moisture cycling of the outer wall layers causes wood-based materials to alternately expand and contract. Repeated moisture cycling often causes warped and bowed boards, delaminated plywood, pushed-out nails, and the separation of wood members from the structure. Moreover, it may also weaken the bond between exterior paint and the substrate material, thereby giving rise to paint failure. In isolated cases, high moisture contents in building materials may cause fungus degradation. Moisture problems in walls have been documented in field surveys carried out by Tsongas (1990), Rose (1986), and Merrill and TenWolde (1989).

Relative to the above discussion, the maximum amount of sorbed (or bound) moisture that can be stored in a material when it is placed in an environment with a relative humidity approaching 100% is denoted "maximum sorption." Liquid water begins to appear in the pore structure of the material when its moisture content approaches and exceeds that of maximum sorption. The condition existing when all pore structures are completely filled with liquid water is called "saturation." For conifer softwoods typically used in building construction, the moisture content at maximum sorption is about 27% of the dry mass of wood and about 230% at saturation. Maximum sorption is generally regarded as the maximum amount of moisture that can be taken on by a material without degradation.

Experts often disagree on the cause and remedial action for moisture problems in residences. A contributing factor to this situation is that general analytical models have not been available to analyze the moisture performance of building components. Mathematical models (e.g., Kohonen [1984], Andersson [1985], Kiessl [1983], Oosterhout and Spolek [1988], and Pedersen [1990]) for predicting time-dependent moisture transfer within building components are currently evolving. Consequently, experimentation and related previous experience are often the only proven approaches available for addressing moisture problems while minimizing heat loss. Experimentation on individual components is, of course, costly and time-consuming. Moreover, specific results cannot be readily extended to different constructions and indoor/outdoor climatic conditions.

Burch et al. (1989) previously presented a distributed moisture capacity, finite-difference model that predicted the time-dependent moisture diffusion in a multilayer wall. This model was one-dimensional and used water vapor pressure as the potential for moisture transfer. The model was experimentally verified for a three-layer wall tested under nonisothermal conditions. This previous model had the limitation that it did not include capillary or convective transfer. In the present paper, the earlier finite-difference model is extended to a more general formulation that includes these effects.

Douglas M. Burch is a mechanical engineer at the National Institute of Standards and Technology, Gaithersburg, MD. **William C. Thomas** is a professor of mechanical engineering, Virginia Polytechnic Institute and State University, Blacksburg.

THEORY

A composite wall composed of N layers in series that stores both heat and moisture is analyzed (see Figure 1). Initially, each layer has an arbitrary moisture content. The exterior surfaces of the wall are then exposed to ambient environments with time-varying temperatures and water vapor pressures. The variation in moisture content and temperature within each of the layers is sought as a function of time. The following assumptions are used in the analysis:

- The driving forces for moisture transfer are the gradients in the moisture content and temperature.
- Heat and moisture transfer is one dimensional.
- The heat transfer properties are constant (i.e., not a function of temperature or moisture content).
- The sorption isotherm is based on the average of adsorption and desorption data. Hysteresis and temperature effects on the sorption isotherm are neglected.
- The effects of temperature and hysteresis on the relationship between suction pressure and moisture content are neglected.
- Vapor adsorption at a surface releases the latent heat of vaporization and vice versa.

Additional assumptions are introduced in the development that follows.

Governing Equations

Within each layer, n, of the wall shown in Figure 1, moisture transfer is governed by the following conservation-of-mass equation:[1]

$$\frac{\partial}{\partial y}\left[D_\gamma(\gamma, T)\frac{\partial \gamma}{\partial y}\right] + \frac{\partial}{\partial y}\left[D_T(\gamma, T)\frac{\partial T}{\partial y}\right] = \frac{\partial \gamma}{\partial t}. \quad (1)$$

The selection of moisture content (γ) and temperature (T) as potentials has the advantage that the same mathematical formulation includes both diffusion transfer and capillary transfer, as will be shown later. This formulation is equivalent (as seen later) to using the gradient in vapor pressure as the moisture transfer potential in the diffusion regime and suction pressure in the capillary flow regime, with a single required diffusivity.

Heat transfer is governed by the conservation of energy equation:

$$\frac{\partial}{\partial y}\left[k(\gamma, T)\frac{\partial T}{\partial y}\right] = \rho(C_d + \gamma C_w)\frac{\partial T}{\partial t}. \quad (2)$$

Latent transport of heat is included in the boundary conditions, as will be discussed later. Enthalpy transport by moisture movement within the material layers is generally small and therefore is neglected in the present analysis. The

[1]Symbols are defined in the nomenclature.

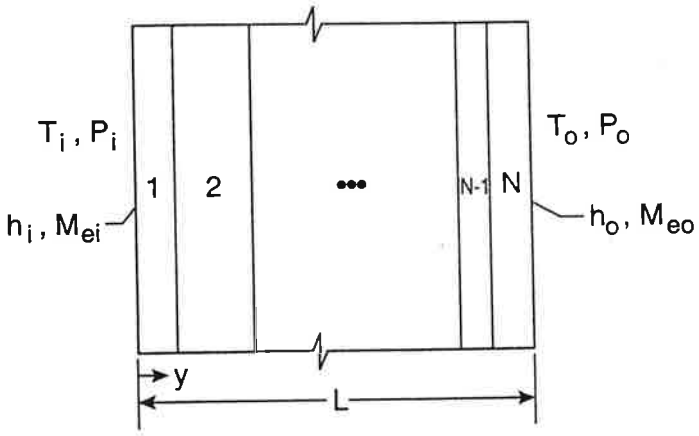

Figure 1 *Wall consisting of* N *layers.*

term $(C_d + \gamma C_w)$ includes the effect of energy storage in both the dry material and accumulated moisture. The effect of accumulated moisture can be important (e.g., the specific heat of wood is increased by 69% after it adsorbs moisture from air at a relative humidity of 100%).

In the above two governing equations, strong couplings exist between heat and moisture transfer. Both the diffusivity for the moisture gradient (D_γ) and the diffusivity for the temperature gradient (D_T) are strong functions of moisture content and temperature. The thermal conductivity (k) can be a function of moisture content and temperature, but for the present analysis it is assumed to be constant.

Indoor Boundary Conditions

At the left boundary of the multilayer wall of Figure 1, the convective heat transfer from the indoor air plus the latent heat from adsorbed or desorbed water vapor is equated to heat conduction into the surface, giving

$$h_i(T_i - T) + \dot{\eta}_i''\lambda = -k\frac{\partial T}{\partial y} \text{ at } y = 0. \quad (3)$$

At the same boundary, the moisture transferred through an air film and paint layer is equated to moisture transferred into the surface, or

$$M_{ei}(P_i - P) = -\rho_d D_\gamma \frac{\partial \gamma}{\partial y} - \rho_d D_T \frac{\partial T}{\partial y} \text{ at } y = 0. \quad (4)$$

Here, an effective conductance (M_{ei}), defined by

$$\frac{1}{M_{ei}} = \frac{1}{M_{fi}} + \frac{1}{M_{pi}}, \quad (5)$$

has been introduced. The effect of a thin vapor retarder, such as paint or a vinyl covering, is taken into account as a surface conductance (M_{pi}) in series with the convective mass transfer coefficient (M_{fi}) associated with the air film.

In Equation 4, the sorption isotherm function (f), defined below, is used as a constitutive relation to evaluate the boundary condition:

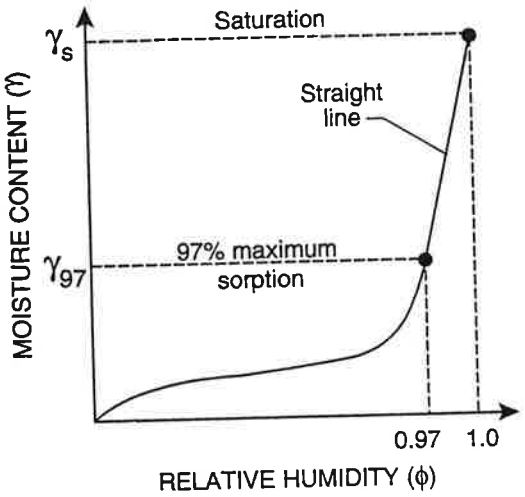

Figure 2 *The sorption isotherm.*

$$\gamma = f(\phi, T) \approx f(\phi) = f\left[\frac{P_v}{P_g}\right]. \tag{6}$$

A sorption isotherm is illustrated in Figure 2. The moisture content of a porous material at a relative humidity of 97% may be measured and is therefore known. Moreover, when a porous material is fully saturated with liquid water, the relative humidity within the pore structure is 100%. When less than fully saturated with water, the relative humidity is less than 100% due to the presence of curved menisci within the pore structure. For the present analysis, a straight line is used to connect the moisture contents just above maximum sorption (ϕ = 97%) and the state of saturation (ϕ = 100%).

Outdoor Boundary Conditions

Similarly, at the right boundary shown in Figure 1, the boundary conditions for heat and moisture transfer are

$$h(T - T_o') + \dot{\eta}_o'' \lambda = -k\frac{\partial T}{\partial y} \quad \text{at } y = L \tag{7}$$

and

$$M_{eo}(P - P_o) = -\rho_d D_\gamma \frac{\partial \gamma}{\partial y} - \rho_d D_T \frac{\partial T}{\partial y} \quad \text{at } y = L. \tag{8}$$

These boundary conditions are evaluated in a fashion similar to those at the indoor surface given in Equations 3 and 4.

Interface between Two Storage Layers

When the heat transfer at the interface between two storage layers is evaluated, the temperature is assumed to be continuous. When the moisture transfer is evaluated, the relative humidity is assumed to be continuous, and the sorption isotherm function (f), illustrated in Figure 2, provides the constitutive relationship, or

$$\phi = f_n^{-1}(\gamma_n) = f_{n+1}^{-1}(\gamma_{n+1}) \tag{9}$$

where the subscripts n and $n+1$ refer to the adjoining regions. The relative humidity is continuous at an interface, but the moisture content will generally be discontinuous.

Nonstorage Layer

The mathematical model has the provision for including nonstorage layers (e.g., an air space, a glass-fiber insulation cavity, or a vapor retarder) that are sandwiched between two storage layers. In a nonstorage layer, the storage of heat and moisture is neglected, and the transfers are steady. A nonstorage layer may be convectively coupled to indoor and outdoor air.

Consider the nonstorage layer shown in Figure 3. At the interface between the nonstorage layer and the adjacent storage layer to the right, the heat transferred through the nonstorage layer plus the heat gains by convective exchange with the indoor and outdoor air and the latent heat from adsorbed or desorbed water vapor are equated to the heat conduction into the storage layer, or

$$\frac{T_{s,n-1} - T_{s,n}}{R} + \dot{V}_i C \rho_a (T_i - T_{s,n}) + \dot{V}_o C \rho_a (T_o - T_{s,n}) + \dot{n}_s'' \lambda = -k\frac{\partial T}{\partial y} \quad \text{at } y = y_s. \tag{10}$$

For the moisture, the diffusion transfer through the nonstorage layer plus the moisture gains due to convective exchange with the indoor and outdoor air are equated to the moisture transfer into the storage layer, or

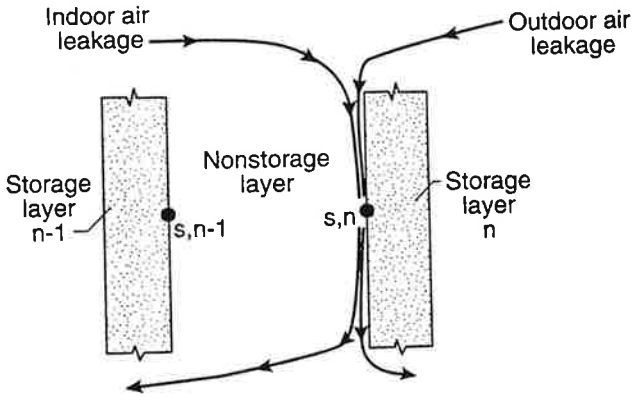

Figure 3 *A nonstorage layer.*

$$M(P_{s,n-1} - P_{s,n}) + \frac{0.622\dot{V}_i\rho_a}{P_a}(P_i - P_{s,n}) + \frac{0.622\dot{V}_o\rho_a}{P_a}(P_o - P_{s,n}) = -\rho_d D_\gamma \frac{\partial \gamma}{\partial y} - \rho_d D_T \frac{\partial T}{\partial y} \quad \text{at } y = y_s. \tag{11}$$

The sorption isotherm function (f) given in Equation 6 is used as a constitutive relation in evaluating the above equation.

Solution Procedure

Equations 1 through 11 were recast into finite-difference equations using a uniform nodal spacing within each layer. An implicit solution technique with coupling between the two conservation equations was used to solve the equations. A Fortran 77 computer program with a tridiagonal-matrix solution algorithm was prepared. At each time step, the calculation proceeds by first solving for the temperature distribution. Next, a set of surface moisture contents is calculated, followed by a set of the interior moisture contents. Next, a revised set of surface moisture contents and interior moisture contents is calculated based on the new values of the diffusion coefficients and so forth. This process is repeated until convergence of the moisture contents is attained. By choosing a sufficiently small time step, the need to iterate between the temperature and moisture solutions was eliminated.

The accuracy of the numerical solution depends on both the nodal spacing and the time step. Progressively smaller nodal spacings and time steps were used to ensure that calculated results did not depend significantly on the space or time increment.

Later in the paper, the program is used to analyze the moisture transfer in a wood-frame wall. For this analysis, a time step of one hour is used. The number of nodes was three in the gypsum board, five in the sheathing, and five in the wood siding. The insulation was treated as a nonstorage layer. When the computer program was run on a personal computer equipped with a math coprocessor and having a 33-Mhz clock speed, 30 minutes of calculation time was required to simulate one year of real time.

MATERIAL PROPERTIES

Heat Transfer Properties

The thermal conductivity, density, and specific heat for the various building materials used in the analysis were taken from ASHRAE (1989) and are summarized in Table 1. The glass-fiber insulation was treated as a nonstorage layer and was assumed to have a thermal resistance of 1.9 $m^2 \cdot °C/W$. The thermal resistances of kraft paper and the paint layers were neglected because these layers are very thin.

Diffusion Regime

In the regime below maximum sorption, free liquid water is not present in the pore structure. Here the term "free liquid water" denotes water that may be removed by body forces when a material is spun in a centrifuge. It does not include capillary condensation, which is bound in the micropores of the material. Procedures used to obtain sorption isotherms and vapor diffusivities for the materials are discussed below.

Sorption Isotherms The sorption isotherm data used in the analysis were taken from Richards et al. (1992), where sorption isotherm data were fit to an equation of the form

$$\gamma = \frac{a_1\phi}{(1 + a_2\phi)(1 - a_3\phi)}, \tag{12}$$

where a_1, a_2, and a_3 are empirical constants determined by a regression analysis of the measured data. The empirical coefficients are summarized in Table 2, and sorption isotherm curves for the materials are given in Figure 4a.

Moisture Diffusivities The water-vapor diffusivities for the materials are based on permeability measurements carried out by Burch et al. (1992). For each material, a series of permeability cup measurements were carried out. In the measurements, small relative humidity differences were imposed across the specimens, and a functional relationship was established between permeability and the average relative humidity across the specimen. Separate measurements carried out at 24°C and 7°C revealed that temperature had an insignificant effect on permeability. In

TABLE 1
Heat Transfer Properties

Material	Thermal Conductivity W/m·°C	Density kg/m³	Specific Heat J/kg·°C
Plywood	0.115	545	1214
Wood Siding	0.118	365	1633
Gypsum Board	0.160	670	1098
Fiberboard Sh.	0.0663	352	1298

TABLE 2
Empirical Constants for Sorption Isotherm Function

Material	a_1	a_2	a_3
Plywood	0.3441	6.177	0.8283
Wood Siding	0.1936	2.095	0.7687
Gypsum Board	0.02465	9.0750	0.93540
Fiberboard Sh.	2.7136	65.267	0.8684

TABLE 3
Empirical Constants for Permeability Function

Material	a_1	a_2	a_3
Plywood	-30.10	3.2963	2.4391
Wood Siding	-28.68	-0.9198	4.5776
Gypsum Board	-23.47	-1.4799	1.0816
Fiberboard Sh.	-24.09	0.1836	-0.3919

this study, the permeability data were fit to an equation of the form

$$\mu = \exp(a_1 + a_2\phi + a_3\phi^2), \tag{13}$$

where a_1, a_2, and a_3 are empirical constants determined from a fit of the measured data. The empirical coefficients are summarized in Table 3. A plot of the permeabilities for the materials used in the analysis is given in Figure 4b.

The diffusivities for the moisture gradient (D_γ) and for the temperature gradient (D_T) were calculated by the relations

$$D_\gamma = \frac{\mu(\phi)\, P_{vg}(T)}{\rho_d \dfrac{\partial f(\phi)}{\partial \phi}}$$

and

$$D_T = \frac{\mu(\phi)\,\phi \dfrac{\partial P_{vg}(T)}{\partial T}}{\rho_d}. \tag{14}$$

The above equations may be derived by introducing the sorption isotherm function and applying the chain rule to Fick's steady-state diffusion equation with the gradient of the water vapor pressure as the driving-force potential.

The glass-fiber insulation, the 19-mm-wide air space, the paint layers, and the kraft paper vapor retarder were treated as nonstorage layers. Permeances for these materials are based on ASHRAE (1989) and are given in Table 4.

Capillary Regime

Capillary transfer occurs when a contiguous path of liquid exists within the porous material. As the moisture content of a material is increased above maximum sorption, the moisture content at which a contiguous path of liquid first exists is termed "irreducible saturation."

Liquid Diffusivity In the capillary flow regime, the liquid diffusivity in porous materials may be predicted by

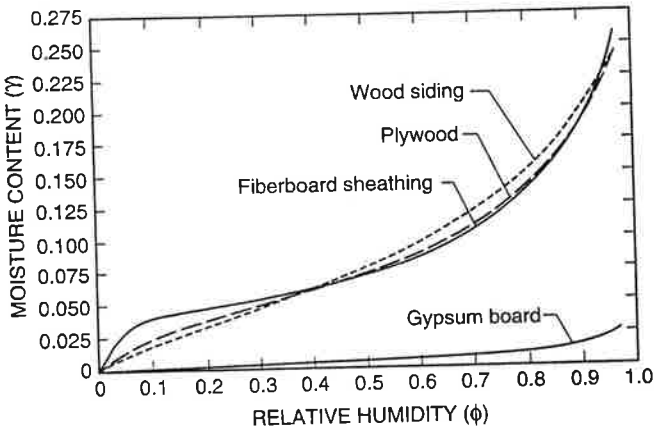

(a) sorption isotherms

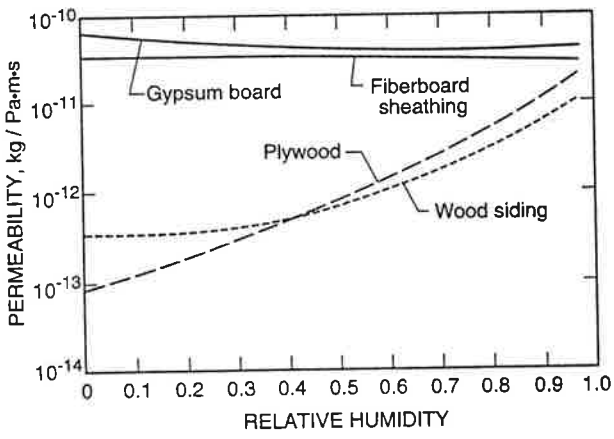

(b) permeabilities

Figure 4 *Diffusion properties of materials used in the analysis.*

TABLE 4 Permeances for Nonstorage Layers	
Material	10^{-10} kg/s·m²·Pa
Latex Paint	5.7
Oil-Based Paint	1.1
92-mm Glass Fiber Ins.	18.
Kraft Paper (Asphalt Impreg.)	0.17
19-mm Air Space	69.

TABLE 5 Dry Porosity and Saturated Liquid Permeability Values Used in Analysis		
Material	ϵ_d	κ_s m²
Plywood	0.636	1.4×10^{-20}
Wood Siding	0.756	2.8×10^{-19}
Fiberboard Sh.	0.765	3.9×10^{-15}

$$D_\gamma = -\frac{\rho_w \kappa \dfrac{\partial P_c}{\partial \gamma}}{\rho_d \nu}. \tag{15}$$

This equation follows by applying the chain rule to Darcy's law for liquid flow through a porous media. In the analysis, the density of water (ρ_w) was taken to be 1,000 kg/m³, and the viscosity of water (ν) was taken to be 7.25×10^{-4} Pa·s. Procedures to obtain the capillary pressure (P_c) and the unsaturated liquid permeability (κ) are discussed below.

Capillary Pressure The Leverett "*j*-function" (Leverett 1941) is accepted by various authors in different fields as a generalized dimensionless functional form that may be used to correlate the capillary pressure with moisture content for many different materials. The Leverett *j*-function is defined as

$$j = \frac{P_c}{\sigma}\sqrt{\frac{\kappa_s}{\epsilon_d}}, \tag{16}$$

where κ_s is the liquid permeability of the porous material at a saturated moisture content and σ is the surface tension of water, taken as 69.2×10^{-3} N/m. Dry porosity (ϵ_d) and saturated liquid permeability values (κ_s) used in the analysis are given in Table 5.

The Leverett *j*-function, or the dimensionless capillary pressure, is plotted as a function of the saturation of the wetting fluid in Figure 5. Here the saturation of the wetting fluid (S) is defined as

$$S = \frac{\gamma - \gamma_{ir}}{\gamma_s - \gamma_{ir}}. \tag{17}$$

The Leverett *j*-function was curve-fitted to data as shown in Figure 5.

Unsaturated Liquid Permeability The unsaturated liquid permeability (κ) was estimated by the linear relation

$$\kappa = \kappa_s S. \tag{18}$$

The above equation is based on the modeling work of Stanish et al. (1985). Note that the unsaturated liquid permeability is equal to zero at irreducible saturation and equal to the saturated liquid permeability (κ_s) at a fully saturated state.

The liquid diffusivity was calculated from Equation 15 using the above procedures to estimate the derivative of the capillary pressure and the unsaturated permeability. The authors recognize that this procedure provides only engineering estimates for the liquid diffusivity of materials. However, liquid diffusivity data for building materials are seriously lacking in the literature. The National Institute of Standards and Technology (NIST) is currently measuring liquid diffusivities for building materials. As these measurement results become available, they will be incorporated into the model and replace the approximate method outlined above.

Within the capillary flow regime, the diffusivity for the temperature gradient (D_T) was calculated using Equation 14.

Transition Regime

When the moisture content of a material is between a state of maximum sorption and irreducible saturation, the

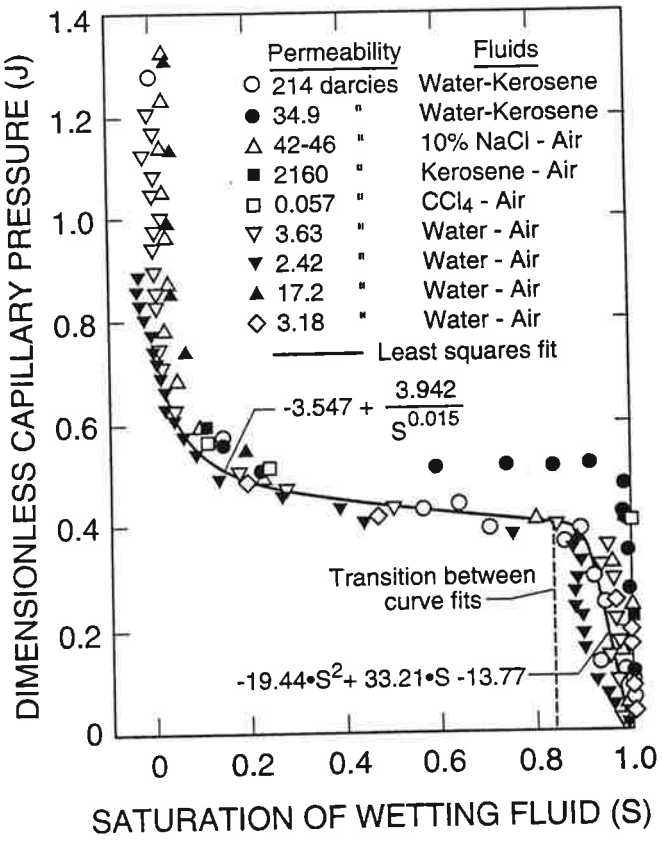

Figure 5 *Dimensionless capillary pressure versus saturation of wetting fluid for unconsolidated sands (Collins 1961).*

material is said to be in a "transition regime." At and below the irreducible saturation moisture content, free liquid water exists but not in a contiguous path. In this regime, the capillary attraction between discrete liquid particles and pores is so strong that this liquid cannot be separated from the porous material by ordinary mechanical means, such as centrifuging or applying a pressure gradient across the material. In this regime, capillary transfer vanishes and the water vapor pressure approaches saturation.

To date, different researchers do not agree on the exact moisture transfer mechanism, especially in an isothermal situation. The present model uses moisture concentration and temperature gradients as the moisture transfer potential in this regime. The diffusivity for the moisture gradient (D_γ) was estimated as a function of moisture content by joining the diffusivity curves in the diffusion and capillary regimes with a straight line (on a logarithmic scale), as shown in Figure 6a. The mathematical relationship for the diffusivity in the transition region is then

$$D_\gamma = D_{ms^-} \exp\left[\frac{\gamma - \gamma_{ms^-}}{\gamma_{ir^+} - \gamma_{ms^-}} \ln\left(\frac{D_{ir^+}}{D_{ms^-}}\right)\right]. \quad (19)$$

In the above equation, D_{ms-} is the left-hand limit of diffusivity at maximum sorption and D_{ir+} is the right-hand limit of liquid diffusivity at irreducible saturation. Note that Equations 14, 15, and 19 provide a continuous model for the moisture diffusivity from a dry to a saturated state. The diffusivity for the temperature gradient (D_T) was also calculated by Equation 14 and is shown in Figure 6b.

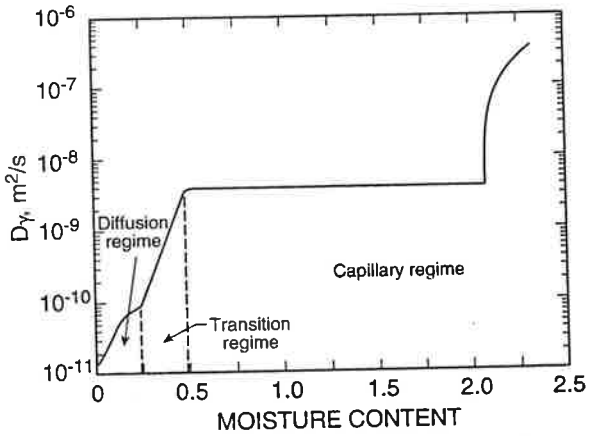

(a) diffusivity for the moisture content gradient

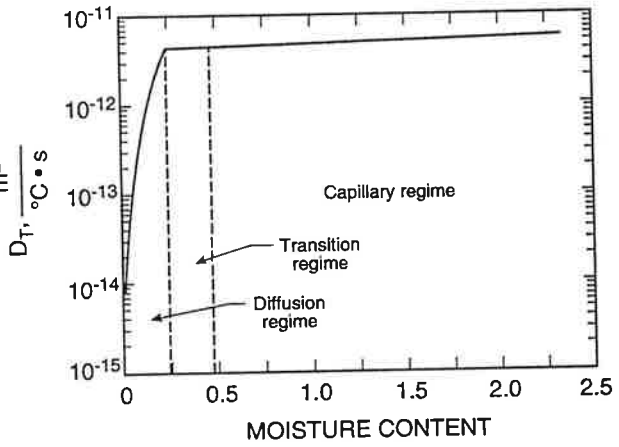

(b) diffusivity for the temperature gradient

Figure 6 *Moisture diffusivity for white pine.*

DISCUSSION OF RESULTS

The above mathematical model was used to predict the seasonal variation in the moisture content of the sheathing and wood siding of the wood-frame wall shown in Figure 7. This wall was composed of 13-mm-thick gypsum board covered with latex paint, 92-mm-thick glass-fiber insulation, 13-mm-thick fiberboard sheathing, and 13-mm-thick wood siding covered with oil-based paint.

In the analysis, the indoor temperature was maintained at 21°C. The outdoor temperature, relative humidity, and solar radiation were taken from WYEC hourly weather data (Crow 1981) for a mild winter climate (Atlanta, Ga.), an intermediate winter climate (Boston, Mass.), and a cold winter climate (Madison, Wis.). The heating degree-days for these cities are 1706°C·days for Atlanta, 3207°C·days for Boston, and 4228°C·days for Madison. Weekly average outdoor temperatures for these three cities are given in Figure 8. Six months of weather data were used to initialize the simulation results so that they would be independent of assumed initial moisture content and temperature.

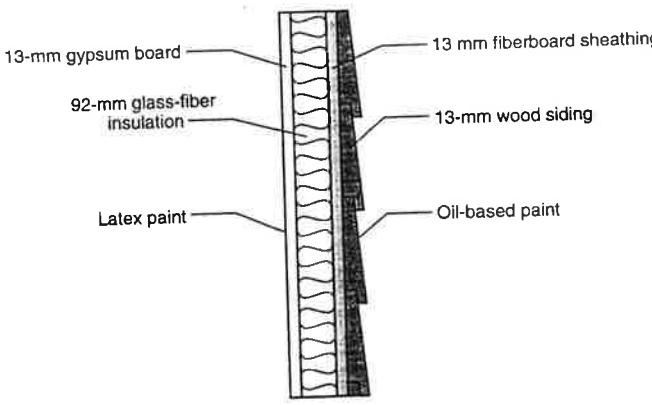

Figure 7 *Wood-frame wall used in the analysis.*

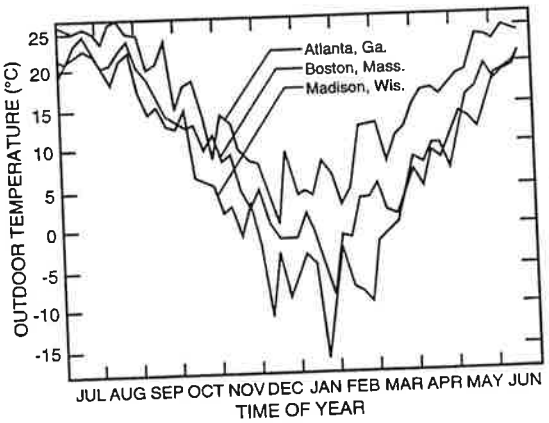

Figure 8 *Weekly average outdoor temperature for the three climates.*

Airtight Wall without a Vapor Retarder

Winter moisture accumulation in an airtight (i.e., no convection) wood-frame wall without a vapor retarder is plotted versus time of year in Figure 9a for an indoor relative humidity of 35% and in Figure 9b for an indoor relative humidity of 50%. In each plot, the solid line depicts the average moisture content of the wood siding, while the broken line depicts the average moisture content of the fiberboard sheathing. In the figures, maximum sorption for the wood siding is depicted by the solid horizontal lines and that for the sheathing by the dashed horizontal line. As indicated earlier, when the moisture content is above maximum sorption, free liquid water exists within the pores of a material, and serious problems are expected if this condition exists over an extended period.

Comparing the pairs of curves for the three different climates in Figure 9a, higher moisture contents are seen to occur in colder climates. In actual houses, the effect of climate will be less pronounced because the indoor relative humidity in houses tends to decrease in colder climates as a result of increased moisture losses from window condensation and infiltration of drier air. It is also interesting to note that the peak moisture content occurs about two months after the minimum outdoor temperature shown in Figure 8.

Comparing Figures 9a and 9b, indoor relative humidity is seen to be a highly significant parameter affecting winter moisture accumulation. Increasing the indoor relative humidity from 35% to 50% substantially increases the moisture accumulation. When the indoor relative humidity was 35% (see Figure 9a), the moisture contents of the sheathing and wood siding were always below maximum sorption. On the other hand, when the indoor relative humidity was increased to 50% (see Figure 9b), the moisture contents approached maximum sorption in Boston and rose considerably above maximum sorption for four to six months in Madison. These large seasonal variations in moisture content will cause wood-based products to undergo

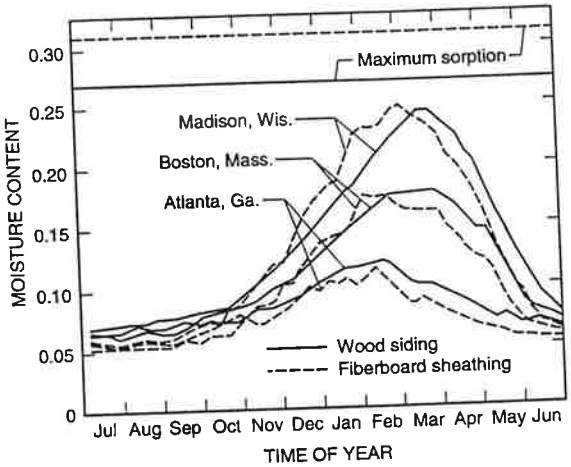

(a) indoor relative humidity, ϕ = 35%

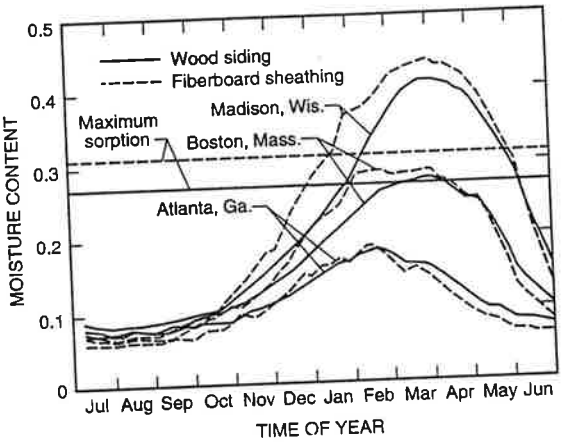

(b) indoor relative humidity, ϕ = 50%

Figure 9 *Moisture content plotted versus time of year for the wood-frame wall without a vapor retarder and without indoor air leakage.*

expansion and contraction cycles that contribute to material degradation.

The results in Figure 9, and with the same type of results following, show that peak moisture accumulation in various materials generally does not exceed maximum sorption by much and, in fact, never reaches the capillary flow regime. This situation means that the overall results are relatively insensitive to the significant uncertainties in material properties above maximum sorption.

Airtight Wall with a Vapor Retarder

A vapor retarder, placed between the gypsum board and the insulation, was added to the wall used in the two previous computer simulations. The vapor retarder consisted of kraft paper having a permeance of 1.7×10^{-11} kg/s·m^2·Pa. The simulation results with this vapor retarder are given in Figure 10 for the same two indoor relative humidity conditions.

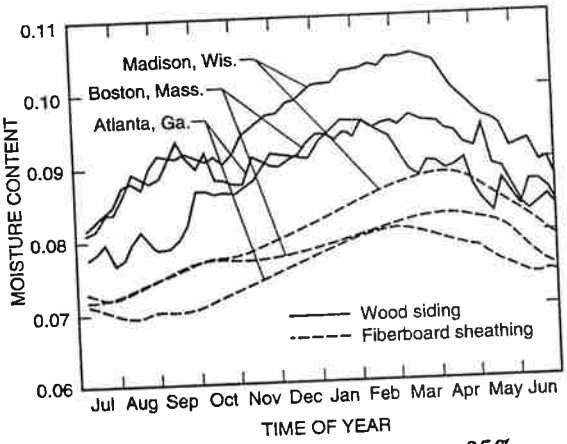

(a) indoor relative humidity, ϕ = 35%

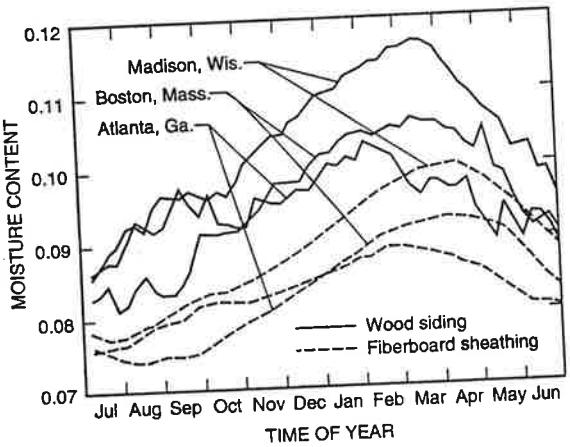

(b) indoor relative humidity, ϕ = 50%

Figure 10 *Moisture content plotted versus time of year for the wood-frame wall with a vapor retarder and without indoor air leakage.*

Comparing Figures 9 and 10, the vapor retarder is seen to provide a significant reduction in the seasonal cycles in moisture content. Note that the moisture content in both the sheathing and the wood siding is always maintained below 12%, even for the higher indoor relative humidity. This reduces the seasonal expansion and contraction cycles in wood-based products, thereby reducing material degradation due to moisture cycling. These results indicate that a vapor retarder is an effective means of controlling moisture accumulation in a wood-frame wall exposed to cold climates.

Wall with a Vapor Retarder and Indoor Air Leakage

The mathematical model was next used to investigate the effect of indoor air leakage on the moisture accumulation within the wood-frame wall with a vapor retarder (see Figure 11). In the analysis, the insulation cavity was ventilated with indoor air at an assumed rate of one volume

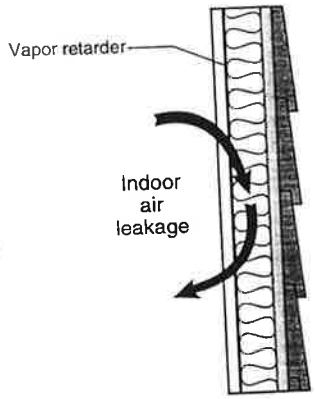

Figure 11 *Illustration of indoor air leakage into insulation cavity of wood-frame wall.*

change per hour. Convective air exchange occurs due to air leakage paths associated with electrical outlet boxes, baseboard cracks, and other inherent penetrations.

The moisture contents of the wood siding and fiberboard sheathing are plotted versus time of year in Figure 12a for an indoor relative humidity of 35% and in Figure 12b for an indoor relative humidity of 50%. For an indoor relative humidity of 50%, the moisture contents are seen to approach maximum sorption in Madison. It should be pointed out that this analysis is one-dimensional and does not include the effect of higher sheathing moisture contents directly in line with impinging air leakage. The effect of convective transport is averaged over the entire sheathing surface.

The results shown in Figure 12 suggest that indoor air leakage is also an important moisture transfer mechanism. Comparing the results of Figures 10 and 12, indoor air leakage is seen to substantially increase the moisture content in a wall with a typical vapor retarder. These results indicate that in order to reduce moisture accumulation in a wood-frame wall exposed to a cold climate, it is also necessary to seal interior air leakage paths.

It should be pointed out that the above analysis is very dependent on an assumed cavity ventilation rate of one volume change per hour. This value was not based on measured data but was rather an engineering estimate that seemed reasonable to the authors.

Effect of Other Construction Parameters

In this section, a sensitivity analysis using the wood-frame wall of Figure 7 is carried out to investigate the effects of orientation, exterior paint permeance, exterior sheathing permeance, and the amount of insulation. In the analysis, the wall is exposed to an indoor relative humidity of 35% and the outdoor weather of Madison, Wis.

Orientation The moisture contents of the sheathing and siding of a north-facing and south-facing wall are compared in Figure 13a. The higher solar radiation for the south-facing wall causes its moisture contents to be lower

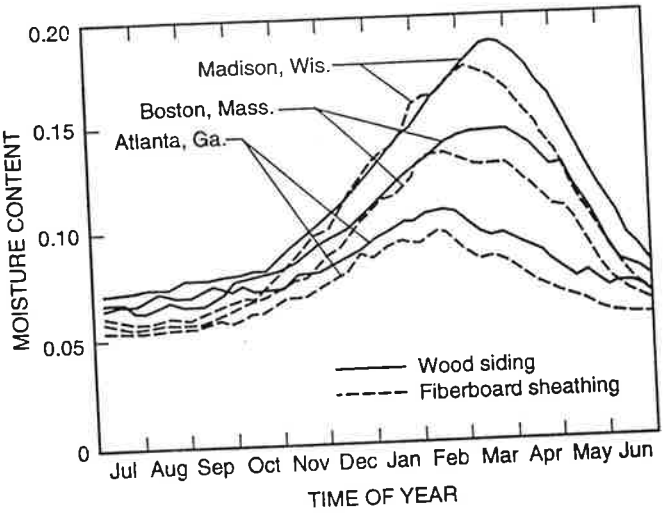

(a) indoor relative humidity, $\phi = 35\%$

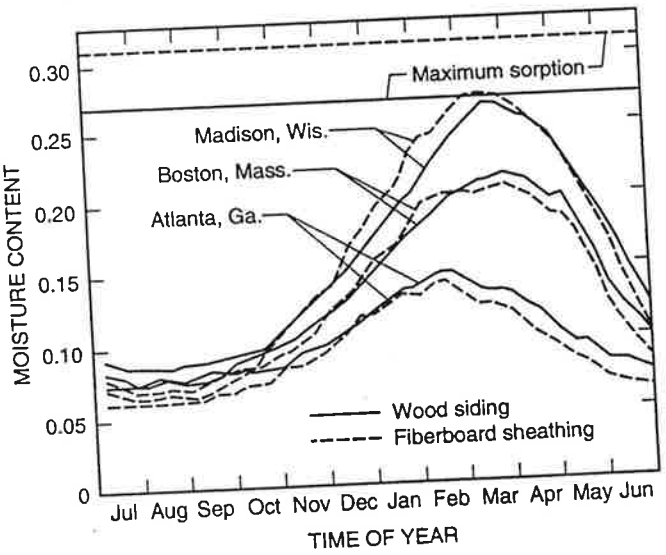

(b) indoor relative humidity, $\phi = 50\%$

Figure 12 *Moisture content plotted versus time of year for the wood-frame wall with a vapor retarder and with indoor air leakage.*

than those of an identical north-facing wall. The peak wood moisture content in the south-facing wall is 0.04 lower than for the identical north-facing wall.

Exterior Paint Permeance In Figure 13b, the moisture accumulation within the wood-frame wall with exterior oil-based paint is compared to the same wall with a considerably more permeable latex paint. The permeance of the latex paint was 5.7×10^{-10} kg/s·m^2·Pa, and that for the oil-based paint was 1.1×10^{-10} kg/s·m^2·Pa.

The results indicate that the use of exterior latex paint, as opposed to oil-based paint, enhances the escape of moisture during warm drying periods and thereby maintains somewhat lower moisture contents in the wood siding. The peak wood moisture content in the wall painted with latex paint is seen to be 0.03 lower than the same wall painted with oil-based paint.

Sheathing Permeance The moisture accumulation for a wood-frame wall with fiberboard sheathing is compared to that for the same wall with the considerably less permeable plywood sheathing. The permeance of the fiberboard sheathing was about 150 times that of the plywood. The results are given in Figure 13c.

The results indicate that the use of less permeable plywood sheathing reduced the ingress of moisture into the wood siding. The peak moisture content in the wood siding for the wall with plywood sheathing was 0.05 lower than that for the same wall with fiberboard sheathing. Note that the moisture content of the two sheathing materials does not differ much.

Amount of Insulation In Figure 13d, the moisture accumulation in a wood-frame wall without insulation is compared to the same wall with insulation. When the thermal insulation is in the wood-frame wall, most of the inside-to-outside temperature difference occurs across the insulation, and a small temperature difference occurs between the sheathing and the wood siding. This causes the moisture content of the sheathing and siding to be not much different. On the other hand, when the thermal insulation is absent from the wall, a much larger temperature difference occurs between the sheathing and the wood siding. This causes moisture to move from the warmer sheathing outward into the colder wood siding. This result indicates that when uninsulated wood-frame walls are retrofitted with thermal insulation in cold climates, the sheathing materials will tend to have an increased moisture content.

Using Outdoor Ventilation as a Moisture Management Technique

Another moisture management technique for wood-frame walls is the use of outdoor ventilation to remove accumulated moisture instead of using an interior vapor retarder and sealing interior air leakage paths. Here a 19-mm naturally ventilated cavity is formed between the sheathing and the wood siding, as shown in Figure 14. In the analysis, the cavity ventilation rate was assumed to be six volume changes per hour.

The results of the analysis are given in Figure 15a for an indoor relative humidity of 35% and in Figure 15b for an indoor relative humidity of 50%. In each figure, the following three cases are compared: the original wood-frame wall shown in Figure 7, the wood-frame wall with an unventilated air cavity, and the wood-frame wall with the ventilated air cavity shown in Figure 14.

These results show that when the sheathing and siding are in contact, the moisture contents of the sheathing and wood siding are not much different. When an unventilated air space is placed between the sheathing and wood siding, the moisture content of the wood siding increases and the moisture content of the sheathing decreases. This effect is caused primarily by the thermal resistance of the air space altering the temperature distribution within the construction

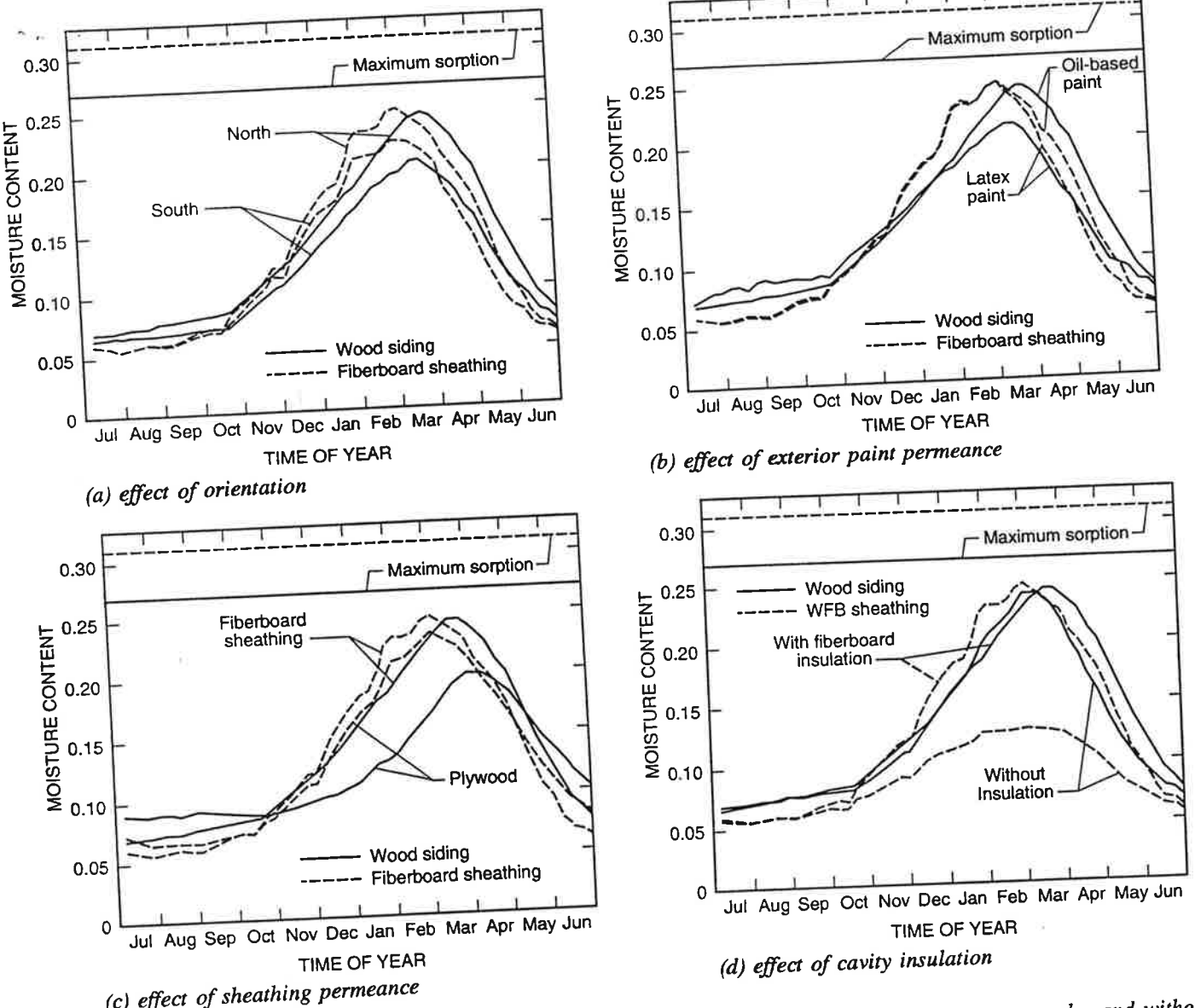

Figure 13 *Moisture content plotted versus time of year for the wood-frame wall without a vapor retarder and without indoor air leakage (Madison, Wis.).*

(i.e., the wood siding becomes colder and the sheathing becomes warmer). The larger temperature difference between the wood siding and the sheathing causes accumulated moisture to redistribute toward the colder wood siding. When the air space is ventilated, the moisture content of both the sheathing and the wood siding decreases.

Comparing Figures 15 and 10, it is seen that the use of outdoor ventilation is considerably less effective in reducing seasonal fluctuations in moisture content than the practice of providing a vapor retarder and sealing air leakage paths at the interior surface.

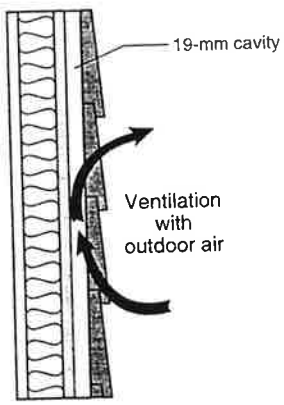

Figure 14 *Illustration of wood-frame wall with an exterior cavity ventilated with outdoor air.*

SUMMARY AND CONCLUSIONS

A mathematical model that predicts the combined transfer of heat and moisture in walls was presented. The

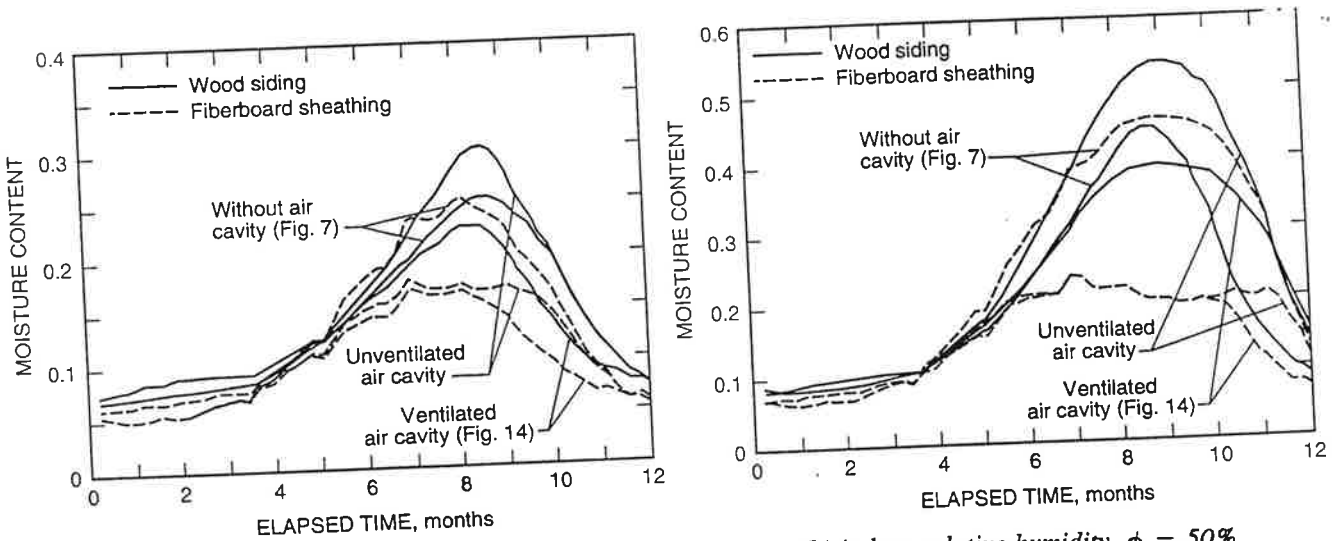

(a) indoor relative humidity, ϕ = 35%

(b) indoor relative humidity, ϕ = 50%

Figure 15 *Comparison of moisture content variation of wood-frame wall without outdoor ventilation (Figure 7) versus that of the wood-frame wall with outdoor ventilation (Figure 14) in Madison, Wis.*

model is one-dimensional and includes diffusion and capillary and convective transfer. The model was used to analyze the winter moisture accumulation in a wood-frame wall exposed to a mild winter climate (Atlanta, Ga.), an intermediate winter climate (Boston, Mass.), and a cold winter climate (Madison, Wis.).

Seasonal changes in outdoor temperature were found to produce seasonal variations in the moisture content of the outer layers of a wood-frame wall. The most important parameters affecting the amount of moisture accumulation during the winter were the indoor relative humidity and the outdoor climate. Indoor relative humidity was observed to be more important than outdoor climate. The amount of moisture accumulation was greater in colder climates. Other parameters found to have a less important effect on moisture accumulation were wall orientation, exterior paint permeance, and sheathing permeance. The addition of insulation to an uninsulated wood-frame wall was found to significantly increase the moisture content of fiberboard sheathing.

Both diffusion and indoor air leakage were shown to be important mechanisms for transporting moisture. In walls without an interior vapor retarder, moisture diffusion was shown to accumulate sufficient moisture to produce free liquid water in the sheathing and wood siding of an airtight wall exposed to an indoor relative humidity of 50% and the outdoor climate of Madison, Wis. The leakage of indoor air into the insulation cavity of a wood-frame wall with an interior vapor retarder was observed to accumulate moisture that approached a state of free liquid water.

The inclusion of a vapor retarder and sealing air leakage paths at the interior wall surface were found to significantly decrease seasonal variations in moisture contents, thereby preventing large expansion and contraction cycles in wood-based products that are believed to degrade the construction. The practice of using outdoor ventilation in a cavity between the sheathing and the siding was found to be less effective than the practice of including a vapor retarder and sealing interior air leakage paths.

ACKNOWLEDGMENTS

The authors thank the Office of Buildings and Community Systems of the Department of Energy for funding this research. The authors would like to acknowledge the helpful discussions with O.A. Plumb on capillary transfer.

NOMENCLATURE

a_n = constants in sorption isotherm and permeability function (n = 1, 2, and 3)
C = specific heat, J/kg·°C
D_γ = diffusivity for moisture gradient, m²/s
D_T = diffusivity for temperature gradient, m²/°C·s
f = sorption isotherm function
h = surface heat transfer coefficient, W/m²·°C
j = dimensionless capillary pressure
k = thermal conductivity of porous material, W/m·°C
L = thickness of wall, m
M = permeance or moisture conductance, kg/s·m²·Pa
P = pressure, Pa
R = thermal resistance, m²·°C/W
S = saturation of wetting fluid (see Equation 17)
t = time, s
T = temperature, °C
T_o' = sol-air temperature, °C
y = distance from inside surface of wall, m
$\dot{V}$ = volumetric airflow rate per unit area, m³/s per m²

ε = porosity
κ = unsaturated liquid permeability, m^2
$\dot{\eta}''$ = moisture mass flux, $kg/m^2 \cdot s$
λ = latent heat of vaporization, J/kg
μ = water vapor permeability, $kg/s \cdot m^2 \cdot Pa$
ν = viscosity of water, Pa·s
ρ = density, kg/m^3
σ = surface tension of water, N/m
ϕ = relative humidity

Subscripts

a = atmospheric or air property
c = capillary
d = dry property
e = effective property
f = air film
g = saturated state
i = indoor or inside surface property
ir = irreducible saturation
ms = maximum sorption
n = storage layer index
o = outdoor property
p = paint property
s = surface value or liquid saturated state
T = temperature gradient
v = vapor property
w = moist or water property
γ = moisture content gradient

REFERENCES

Andersson, A.C. 1985. Verification of calculation methods for moisture transport in porous building materials. Document D6:1985 (ISBN 91-540-4325-5). Stockholm: Swedish Council for Building Research.

ASHRAE. 1989. *1989 ASHRAE handbook—Fundamentals*, ch. 22. Atlanta: American Society of Heating, Refrigerating and Air-Conditioning Engineers, Inc.

Burch, D.M., W.C. Thomas, L.R. Mathena, B.A. Licitra, and D.B. Ward. 1989. Transient moisture and heat transfer in multilayer nonisothermal walls—Comparison of predicted and measured results. *Proceedings of the Conference on the Thermal Performance of the Exterior Envelopes of Buildings IV*, Orlando, FL, December 4-7, pp. 513-531.

Burch, D.M., W.C. Thomas, and A.H. Fanney. 1992. Water vapor permeability measurements of common building materials. *ASHRAE Transactions* 98(2).

Collins, R.E. 1961. *Flow of fluids through porous materials*, pp. 31-33. New York: Reinhold.

Crow, L.W. 1981. Development of hourly data for weather year for energy calculations (WYEC). *ASHRAE Journal* 23(10): 37-41.

Duff, J.E. 1968. Moisture distribution in wood-frame walls in winter. *Forest Products Journal* 18(1).

Kiessl, K. 1983. Kapillarer and dampfformiger feuchtetransport in mehrschichtigen bauteilen. Dissertation zur Erlangung des Grades Doktor-Ingenieur des Fachbereiches Bauwesen der Universitat-Gesamthochschule-Essen.

Kohonen, R. 1984. A method to analyze the transient hygrothermal behavior of building materials and components. Publication 21, Technical Research Centre of Finland, Laboratory of Heating and Ventilation. October.

Leverett, M.C. 1941. Capillary behavior in porous solids. *AIME Transactions* 142: 152-169.

Merrill, J.L., and A. TenWolde. 1989. Overview of moisture-related damage in one group of Wisconsin manufactured homes. *ASHRAE Transactions* 95(1).

Oosterhout, G.O., and G.A. Spolek. 1988. Transient heat and mass transfer in layered walls. *Proceedings of ASME Symposium on Heat and Mass Transfer in Insulation Systems*.

Pedersen, C.R. 1990. Combined heat and moisture transfer in building constructions. Report No. 214. Lyngby: Technical University of Denmark, Thermal Insulation Laboratory.

Richards, R.F., D.M. Burch, and W.C. Thomas. 1992. Water vapor sorption measurements of common building materials. *ASHRAE Transactions* 98(2).

Rose, W.B. 1986. Moisture damage to homes in Champaign, IL. *Proceedings of the Symposium on Air Infiltration, Ventilation, and Moisture Transfer*, pp. 198-211. Ft. Worth, TX, Dec. 2-4.

Stanish, M.A., G.S. Schajer, and F. Kayihan. 1985. Mathematical modeling of wood drying from heat and mass transfer fundamentals. *Proceedings of Drying 1985*. New York: Hemisphere Publications.

Tsongas, G. 1990. The Northwest wall moisture study: A field study of excess moisture in walls and moisture problems and damage in new Northwest homes. Report No. DOE/BP-91489-1. June. Portland, OR: Bonneville Power Administration.